文章编号:1673-9981(2014)02-0097-06

无铅易切削黄铜合金高温热压缩流变应力行为*

甘春雷,郑开宏,王海艳,戚文军,周　楠,蔡　畅

广东省工业技术研究院(广州有色金属研究院),广东 广州　510650

摘　要:在变形温度为823～973 K,应变速率为0.01～1 s^{-1}的条件下,采用热压缩实验研究了无铅易切削黄铜合金的高温流变应力行为,结果表明:在所有变形条件下该合金的流变曲线均出现软化现象,这种流变软化主要是由于发生了动态再结晶和$\beta \to \alpha$相变造成的.基于热压缩试验所得实测数据,建立了材料常数为应变的6次多项式函数的双曲正弦形式的本构模型,与实验数据对比表明,该模型能够较好地预测无铅易切削黄铜合金的流变应力.

关键词:无铅易切削黄铜合金;热变形;流变应力;本构模型

中图分类号:TG146.2　　**文献标识码**:A

随着人们环保意识的增强以及对自身健康的关注,无铅易切削黄铜合金的开发和应用研究逐渐得到重视.相关研究者对无铅易切削黄铜合金开展了广泛的研究[1-4],并取得了一些研究成果.然而,由于无铅易切削黄铜合金在热变形后易出现组织和性能缺陷,极大地限制了其实用性,因此,有必要对无铅易切削黄铜合金的热变形行为进行深入的研究.迄今为止,对无铅黄铜合金的研究主要集中在切削性能、拉伸性能和腐蚀性能等方面[5-7],而对其热变形行为的研究报道较少.

材料在热变形过程中的流变应力通常采用本构方程来进行表征,通过本构方程将流变应力、变形温度和应变速率联系起来,分析材料在热变形过程中的本构特征.目前已有多种流变应力本构模型被用来模拟材料在热变形过程中的流变应力变化情况[8-12].在这些模型中,Sellars C M 等人[13]提出的现象本构模型被广泛用来预测材料的热变形行为.近年来,该模型被进一步修正,发展出了考虑应变补缩的本构模型来模拟不同合金的热变形行为[14-17],对热变形行为的预测更加精确.

本研究以无铅易切削黄铜合金为对象,通过在Gleeble-1500热模拟机上进行圆柱体压缩试验,研究在热压缩变形时,变形温度和应变速率对合金的流变应力的影响,获得无铅易切削黄铜合金在不同变形工艺参数条件下的应力值,建立该合金在高温下变形时的流变应力预测本构模型(考虑应变补缩),为开展无铅易切削黄铜合金加工过程的数值模拟、加工工艺的制订以及成形过程组织性能精确控制提供实验数据和理论基础.

1　实验材料及方法

试验材料为采用普通浇铸方法制备的无铅易切削黄铜合金,其成分为(质量分数,%):Cu-36.3Zn-1.76Mg-0.5Bi-0.5Sb,铸态微观组织如图1所示.采用线切割机,将样品制成直径10 mm,长度15 mm的圆柱体.压缩试验在Gleeble-1500热模拟机上进行.进行压缩试验时,在压头与试样两端接触处夹一层1 mm厚的石墨薄片进行润滑,以减少摩擦对应力及变形状态的影响.设定压缩试验变形温度范围为823～973 K,应变速率范围为0.01～1 s^{-1},总压缩变形量为60%.压缩试验完成后,立即水淬.采用

收稿日期:2014-02-25

*基金项目:广东省部产学研结合项目(No.2012B091100038);广州市科技计划项目(7411804513611);广州有色金属研究院博士启动基金(2012B001)

作者简介:甘春雷(1977-),男,江西南昌人,博士.

LEICA-DMI3000M 型金相显微镜对试样中部进行金相组织观察,所用浸蚀剂配比为:40 mL 硝酸+40 mL 冰醋酸+20 mL 水.

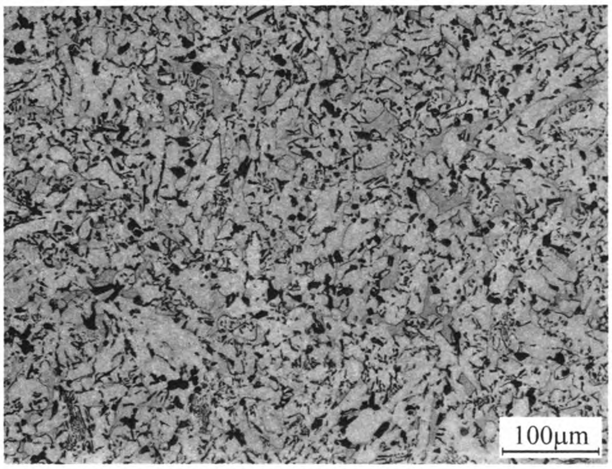

图 1 无铅易切削黄铜合金铸态微观组织

Fig. 1 Microstructure of the as-cast lead-free machinable brass

2 实验结果与讨论

2.1 流变应力变化

通过计算机采集数据,获得无铅易切削黄铜合金压缩变形时的变形温度、应变速率、真应变和流变应力等数据,绘制出在不同条件下,无铅易切削黄铜合金的压缩变形真应力-真应变曲线(图 2). 由图 2 可见:变形温度和应变速率对合金的流变应力具有很大的影响,随着应变速率的增加和变形温度的降低,流变应力增加. 进一步观察可以发现,随着应变的增加,流变应力快速增加到峰值,然后缓慢减少至稳态值,在某些条件下随着应变的增加,流变应力会减少至更低值. 这些特征表明,在本文的试验条件下,无铅易切削黄铜合金在热压缩变形过程中出现了明显的再结晶现象.

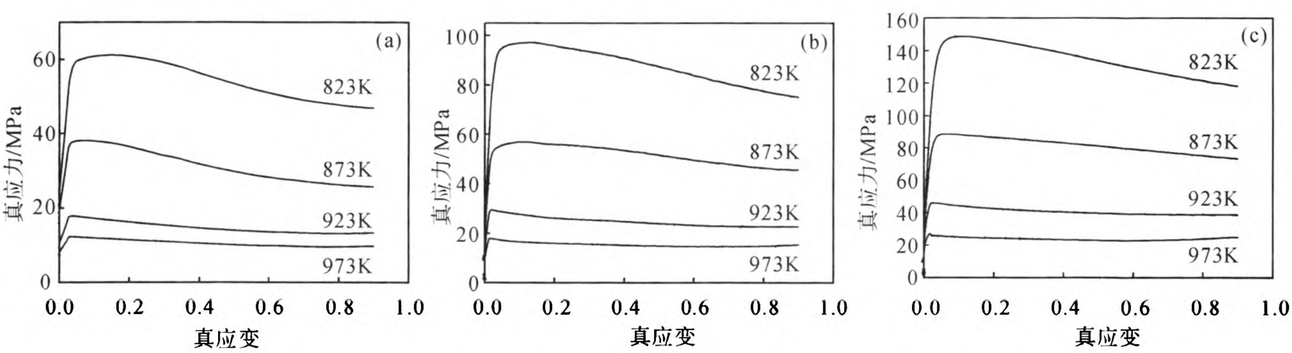

图 2 无铅易切削黄铜合金在温度 823~973 K 和不同应变速率下的真应力-真应变曲线

(a) 0.01 s^{-1};(b) 0.1 $^{-1}$;(c) 1 s^{-1}

Fig. 2 True stress-true strain curves of the lead-free machinable brass alloy in a temperature range of 823-973 K with strain rate of (a) 0.01 s^{-1}, (b) 0.1 s^{-1}, (c) 1 s^{-1}

2.2 微观组织观察

无铅易切削黄铜合金在热变形条件下,其流变应力出现峰值,这与合金中发生了动态再结晶密切相关. 在变形初始阶段,由于加工硬化占主导地位,合金中的硬化作用大大超过软化作用;随变形程度的继续增加,位错密度不断增高,加快了动态回复和动态再结晶,软化作用逐渐增强,使得流变应力达到峰值后开始下降. 这种动态再结晶现象可以通过试样热变形后的微观组织得到证明(图 3). 由图 3 可见,在变形温度为 823 K,应变速率为 1 s^{-1}的条件下,在箭头所指区域内出现了新的尺寸较小的动态再结晶晶粒.

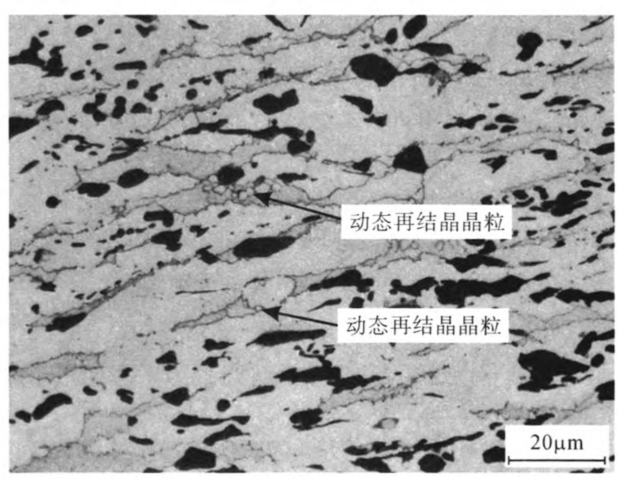

图 3 823 K,1 s^{-1}条件下压缩试样组织

Fig. 3 Microstructure of the compression specimen: 823 K,1 s^{-1}

另外,无铅易切削黄铜合金在热变形条件下出现动态软化与发生了$\beta \to \alpha$相变也有关系.图4是在应变速率0.01～1 s^{-1},温度823～973 K的条件下,合金的典型金相组织照片.由图4可见,在温度低于923 K时,由于试样未完全发生动态再结晶,因而存在再结晶组织和变形带组织共存的现象(见图4(e)).当温度超过923 K时,由于发生了相变,合金的微观组织出现了显著的变化.例如,在变形温度为973K时,出现了细小的针状α相(见图4(d)和(f)).由于α相(面心立方结构)比β相(体心立方结构)具有更好的塑性变形能力,因此,β相增多有利于提高无铅易切削黄铜合金在热变形过程中的变形协调能力,从而降低变形阻力[18].

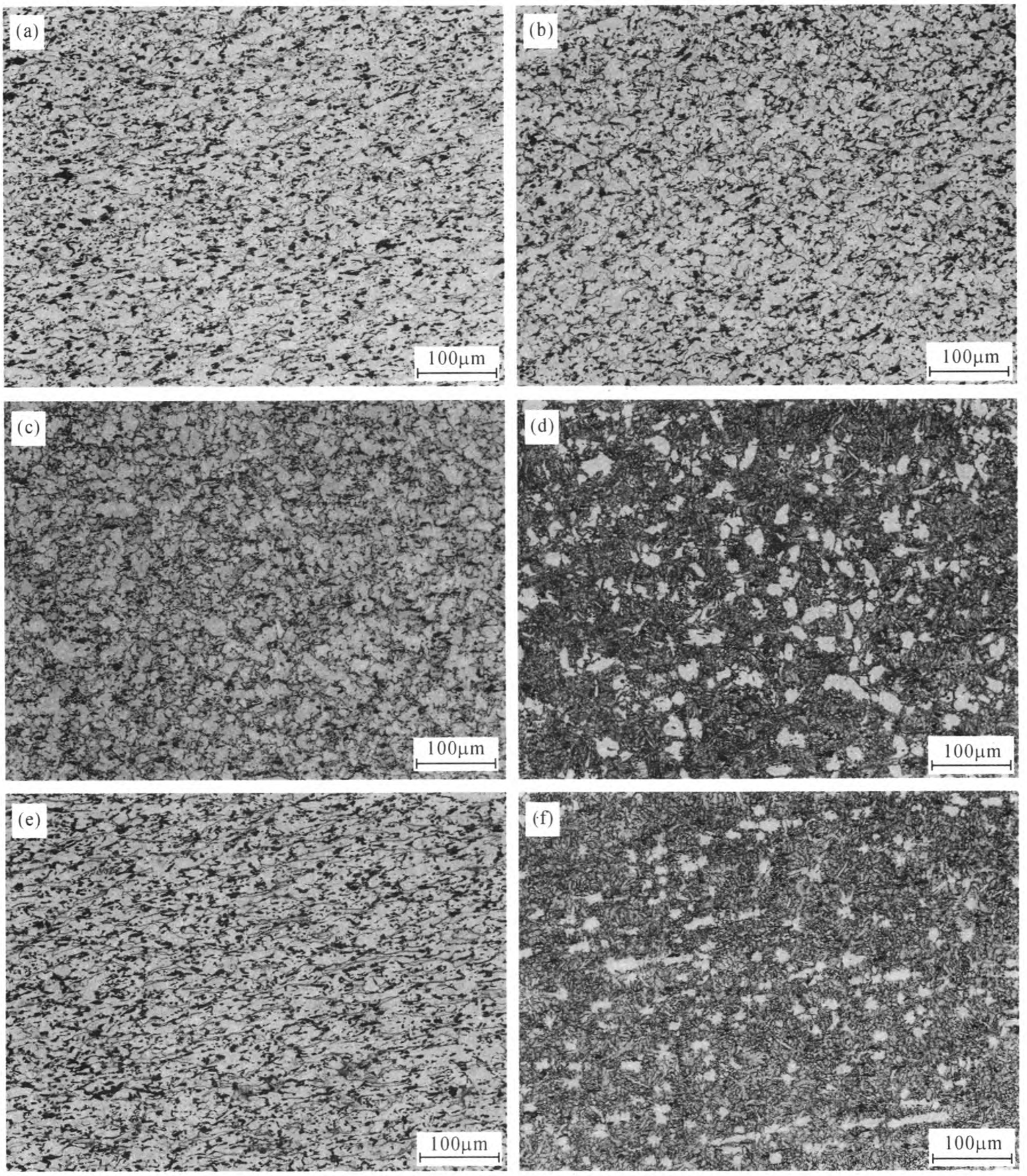

图4　典型的压缩试样微观组织

Fig. 4　Typical microstructures of the compression specimens

(a)823 K,0.01 s^{-1}; (b)873 K,0.01 s^{-1}; (c)923 K,0.01 s^{-1}; (d)973 K,0.01 s^{-1}; (e)823 K,1 s^{-1}; (f)973 K,1 s^{-1}

2.3　流变应力本构模型的建立

从无铅易切削黄铜合金的热压缩流变曲线可知，流变应力的大小取决于变形温度和应变速率，这种力学变形行为可采用 Arrhenius 方程进行描述：

$$\dot{\varepsilon}=AF(\sigma)\exp\left(-\frac{Q}{R_0T}\right). \tag{1}$$

其中：

$$\begin{cases} F(\sigma)=\sigma^{n_1} & \alpha'\sigma<0.8 \\ F(\sigma)=\exp(\beta_1\sigma) & \alpha'\sigma>1.2 \\ F(\sigma)=[\sinh(\alpha'\sigma)]^n & 对所有\sigma. \end{cases} \tag{2}$$

式(1)中，R_0 为气体普式常量，8.314 J/(mol・K)；$\dot{\varepsilon}$ 为应变速率，s^{-1}；σ 为流变应力，MPa，Q 为变形激活能，kJ/mol；T 为变形温度，K；β_1，n_1，α'，n 和 A 为材料常数，$\alpha'=\beta_1/n_1$.

将式(2)中的 $F(\sigma)$ 代入式(1)并求对数得到：

$$\ln\dot{\varepsilon}=n_1\ln\sigma+\ln A_1-Q/R_0T. \tag{3}$$

$$\ln\dot{\varepsilon}=\beta_1\sigma+\ln A_2-Q/R_0T. \tag{4}$$

$$\ln\dot{\varepsilon}=n\ln[\sinh(\alpha'\sigma)]+\ln A-Q/R_0T. \tag{5}$$

热变形条件下通常采用温度补偿的变形速率因子 Zener-Hollomon(Z)参数，有

$$A[\sinh(\alpha'\sigma)]^n=\dot{\varepsilon}\exp\left(-\frac{Q}{R_0T}\right)=Z. \tag{6}$$

得到适用于工艺分析的流变应力模型：

$$\sigma=\frac{1}{\alpha'}\ln\left[\sqrt[n]{\frac{Z}{A}}+\sqrt{\sqrt[n]{\left(\frac{Z}{A}\right)^2}+1}\right]. \tag{7}$$

变形程度对变形激活能和材料常数具有重要的影响，为了提高流变应力模型的预测精度，将材料常数表示成真应变 ε 的多项式函数. 在真应变 0.05～0.85 范围内进行拟合，从 1 至 9 次进行多项式拟合，发现 6 次多项式具有较好的拟合结果(图 5). 获得了如式(8)所示的多项式方程组，式(8)中相应的系数列于表 1.

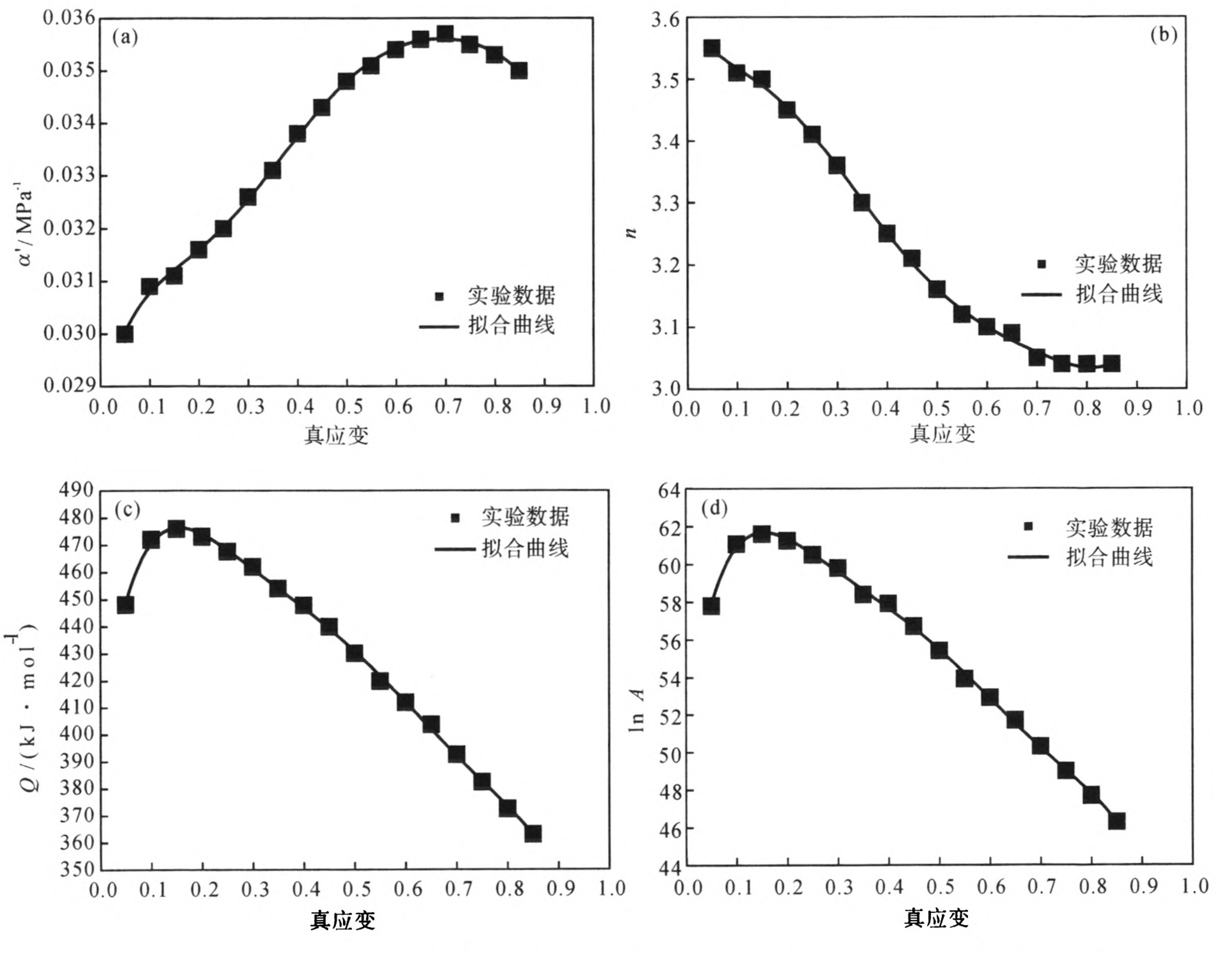

图 5　无铅易切削黄铜合金 6 次多项式拟合获得的(a) α'，(b) n，(c) Q，(d) $\ln A$ 与真应变的关系

Fig.5　Relationships between (a) α', (b) n, (c) Q, (d) $\ln A$ and true strain by sixth polynomial fit of the lead-free machinable brass alloy

$$\begin{cases}\alpha'=\alpha_6\varepsilon^6+\alpha_5\varepsilon^5+\alpha_4\varepsilon^4+\alpha_3\varepsilon^3+\alpha_2\varepsilon^2+\alpha_1\varepsilon+\alpha_0\\ n=n_6\varepsilon^6+n_5\varepsilon^5+n_4\varepsilon^4+n_3\varepsilon^3+n_2\varepsilon^2+n_1\varepsilon+n_0\\ Q=Q_6\varepsilon^6+Q_5\varepsilon^5+Q_4\varepsilon^4+Q_3\varepsilon^3+Q_2\varepsilon^2+Q_1\varepsilon+Q_0\\ \ln A=A_6\varepsilon^6+A_5\varepsilon^5+A_4\varepsilon^4+A_3\varepsilon^3+A_2\varepsilon^2+A_1\varepsilon+A_0.\end{cases} \tag{8}$$

表 1　α', n, Q 和 $\ln A$ 的多项式拟合系数

Table 1 Coefficients of the polynomial for α', n, Q and $\ln A$

α' 的系数	n 的系数	Q 的系数	$\ln A$ 的系数
$\alpha_6=-0.48997$	$n_6=38.04909$	$Q_6=-11407.32565$	$A_6=-1792.5547$
$\alpha_5=1.47391$	$n_5=-103.87566$	$Q_5=34964.06439$	$A_5=5371.34169$
$\alpha_4=-1.71823$	$n_4=106.72796$	$Q_4=-42623.66137$	$A_4=-6399.52548$
$\alpha_3=0.94854$	$n_3=-49.23153$	$Q_3=26362.92331$	$A_3=3869.84795$
$\alpha_2=-0.25085$	$n_2=9.47085$	$Q_2=-8787.44022$	$A_2=-1262.04895$
$\alpha_1=0.03859$	$n_1=-1.33644$	$Q_1=1365.08834$	$A_1=192.86609$
$\alpha_0=0.02863$	$n_0=3.59658$	$Q_0=399.43798$	$A_0=50.9341$

为了验证所建立的流变应力模型的可靠性，采用相关系数 R 和平均绝对误差 $AARE$ 进行表征：

$$R=\frac{\sum_{i=1}^{k}(\sigma_{\exp}^{i}-\bar{\sigma}_{\exp})(\sigma_{\mathrm{pre}}^{i}-\bar{\sigma}_{\mathrm{pre}})}{\sqrt{\sum_{i=1}^{k}(\sigma_{\exp}^{i}-\bar{\sigma}_{\exp})^2\sum_{i=1}^{k}(\sigma_{\mathrm{pre}}^{i}-\bar{\sigma}_{\mathrm{pre}})^2}}. \tag{9}$$

$$AARE(\%)=\frac{\sum_{i=1}^{k}\frac{|\sigma_{\mathrm{pre}}^{i}-\sigma_{\exp}^{i}|}{\sigma_{\exp}^{i}}}{k}\times 100. \tag{10}$$

式(9)和式(10)中，k 为总的数据，$\sigma_{\exp}$ 为实验值，σ_{pre} 为流变应力模型的预测值，$\bar{\sigma}_{\exp}$ 和 $\bar{\sigma}_{\mathrm{pre}}$ 分别为 $\sigma_{\exp}^{i}$ 和 $\sigma_{\mathrm{pre}}^{i}$ 的平均值. 由式(9)计算出相关系数 $R=0.99815$ (图 6)，由式(10)计算出平均绝对误差 $AARE=6.105\%$，表明基于 Arrhenius 方程构建的流变应力模型具有较好的预测精度.

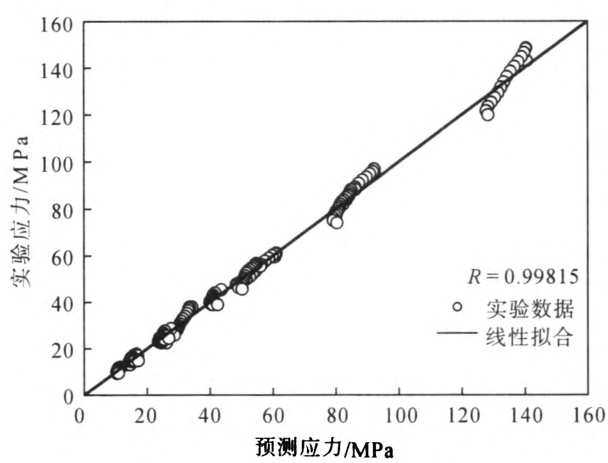

图 6　流变应力预测值与实验值比较

Fig.6 Correlation between predicted and experimental stresses

3 结　论

(1)无铅易切削黄铜合金热压缩流变应力随应变速率的减小和变形温度的增加而减小，其相互关系可用 Z 参数进行表征.

(2)由金相组织观察可知，在应变速率为 0.01～1 s^{-1} 的条件下，当变形温度低于 923 K 时发生动态再结晶，在变形温度超过 923 K 时发生 $\beta\rightarrow\alpha$ 相变，这两种作用使流变应力出现动态软化.

(3)所建立的无铅易切削黄铜合金流变应力模型的相关系数为 0.99815，平均绝对误差为 6.105%，表明该模型具有较好的预测精度.

参考文献：

[1] MOHAMED A T, NAHED A E, RAWIA M H, et al. Machinability characteristics of lead free-silicon brass alloys as correlated with microstructure and mechanical properties[J]. Ain Shams Engineering Journal, 2012, 3(4): 383-392.

[2] LI S F, KONDOH K, IMAI H, et al. Fabrication and properties of lead-free machinable brass with Ti additive by powder metallurgy[J]. Powder Technology, 2011, 205(1-3): 242-249.

[3] TOSHIKAZU M, TAKAYUKI O. Cutting of lead-free copper alloy "Eco Brass"[J]. Journal of Japanese Research Institute Advanced Copper-Base Material Technology, 2006, 45: 250-255.

[4] EMELINA N B, ALABIN A N, BELOV N A. Influ-

ence of bismuth and lead on the formation of the structure of experimental alloys with a Cu-30%Zn based composition during crystallization, deformation, and thermal treatment[J]. Russian Journal of Non-ferrous Metals, 2010,51(6):476-482.

[5] XIAO L R, SHU X P, YI D Q, et al. Microstructure and properties of unleaded free-cutting brass containing stibium[J]. Trans Nonferrous Met Soc China, 2007, 17: 1055-1059.

[6] ATSUMI H, IMAI H, LI S F, et al. High-strength, lead-free machinable-duplex phase brass Cu-40Zn-Cr-Fe-Sn-Bi alloys[J]. Materials Science and Engineering A, 2011, 529:275-281.

[7] YOU S J, CHOI Y S, KIM J G, et al. Stress corrosion cracking properties of environmentally friendly unleaded brasses containing bismuth in Mattsson's solution[J]. Materials Science and Engineering A, 2003, 345: 207-214.

[8] MOMENI A, DEHGHANI K. Characterization of hot deformation behavior of 410 martensitic stainless steel using constitutive equations and processing maps[J]. Materials Science and Engineering A, 2010, 527(21-22): 5467-5473.

[9] XIAO M L, LI F G, ZHAO W, et al. Constitutive equation for elevated temperature flow behavior of TiNi-Nb alloy based on orthogonal analysis[J]. Materials and Design, 2012, 35:184-193.

[10] SHI L, YANG H, GUO L G, et al. Constitutive modeling of deformation in high temperature of a forging 6005A aluminum alloy [J]. Materials and Design, 2014, 54: 576-581.

[11] GAO L, LUO A A. Hot deformation behavior of as-cast Mg-Zn-Mn-Ce alloy in compression[J]. Materials Science and Engineering A, 2013, 560: 492-499.

[12] LIN Y C, DING Y, CHEN M S, et al. A new phenomenological constitutive model for hot tensile deformation behaviors of a typical Al-Cu-Mg alloy[J]. Materials and Design, 2013, 52:118-127.

[13] SELLARS C M, MCTEGART W J. On the mechanism of hot deformation[J]. Acta Metallurgical, 1996, 14(9):1136-1138.

[14] MIRZAEI A, ZAREI-HANZAKI A, HAGHDADI N, et al. Constitutive description of high temperature flow behavior of Sanicro-28 super-austenitic stainless steel [J]. Materials Science and Engineering A, 2014, 589: 76-82.

[15] ZHONG J, XIAO Y H, GUO C. Constitutive modelling for high temperature behaviour of 12CrNiMoWV martensitic stainless steel[J]. Materials Science Technology, 2012, 28(6):719-726.

[16] YIN F, HUA L, MAO H J, et al. Constitutive modeling for flow behavior of GCr15 steel under hot compression experiments[J]. Materials and Design, 2013, 43:393-401.

[17] LUAN J, SUN C, LI X, et al. Constitutive model for AZ31 magnesium alloy based on isothermal compression test[J]. Materials Science Technology, 2014, 30 (2):211-219.

[18] XIAO Y H, GUO C, GUO X Y. Constitutive modeling of hot deformation behavior of H62 brass[J]. Materials Science and Engineering A, 2011, 528(21): 6150-6158.

Flow stress behavior of lead-free machinable brass during high-temperature compression deformation

GAN Chunlei, ZHENG Kaihong, WANG Haiyan, QI Wenjun, ZHOU Nan, CAI Chang

Guangdong General Research Institute for Industrial Technology (Guangzhou Research Institute of Non-ferrous Metals), Guangzhou 510650, *China*

Abstract: The hot deformation behaviors of the newly developed lead-free machinable brass are investigated by isothermal compression tests on a Gleeble-1500 thermal-mechanics simulator at temperatures of 823－973 K and strain rates ranging from 0.01 to 1 s^{-1}. The typical flow curves exhibit softening at all the deformation conditions, which have been considered that the flow softening results from (下转第 107 页)

An investigation of ceryl powder injection molding binder

CHEN Qiang, LI Dandan, CIA Yixiang, TAN Lixin

Guangdong General Research Institute for Industrial Technology (Guangzhou Research Institute of Nonferrous Metals) Guangzhou 510650, *China*

Abstract: By improving the binder of injecting molding composed of PW, PE(polyethylene) and PP(polypropylene), PP (polypropylene) was replaced with EVA(ethylene-acetic acid vinyl ester) and new binder was investigated taking the paraffin(PW) as the principal thing of the binder of injecting molding. The test results showed that the powder filling amount increased from 54% to 60% and the plasticizing time decreased to one tenth of primary time after improving binder; also the twice pouring feed could note shape better, the performance of feed was improved entirely; injection cycle shortened from 120-150 s to 36-42 s; the rate of final products increased from 75% to more than 98%; it is easy to control degrease and sintering deformation, the dimensional precision is controlled about 0.40%.

Key words: injection molding; binder; powder filling lever

(上接第 102 页)the occurrence of DRX behavior and the $\beta \rightarrow \alpha$ phase transformation of the lead-free machinable brass. On the basis of the experimental data, a new constitutive model with the material constants expressed by a sixth order polynomial fitting of strain was developed through a hyperbolic-sine Arrhenius type equation to relate the flow stress, strain rate and temperature. The flow stresses calculated by the proposed constitutive model are good agreement with the experimental ones.

Key words: lead-free machinable brass; hot compression deformation; flow stress; constitutive model